

FEM non-linear modelling of cob using ANSYS

***†Jimenez Alejandro¹, O'Dwyer Dermot¹**

¹Department of Civil Structural and Environmental Engineering, Trinity College Dublin, Ireland.

*†Presenting & Corresponding author: jimnezra@tcd.ie

Abstract

Cob is an earthen construction technique used to build monolithic load-bearing walls. Mainly of vernacular nature, remaining cob buildings can be found throughout Europe as well as in other specific locations around the world.

The aim of this paper is to evaluate the available material models' suitability for the modelling of cob's structural behavior in one of the most commonly used FEM software in the market. The stress-strain graphs obtained and the failure mechanisms observed after a simple compression and diagonal compression experimental campaign in cob wallettes were replicated using three different material constitutive models, namely, MISO, CONCR, and DMGE/DMGI. Furthermore, a mesh size sensitivity analysis was performed following a mesh refinement approach.

MISO could reproduce the pre-peak behavior of cob and principal stresses could be used as an indication of the opening of cracks. On the other hand, it did not capture the softening post-peak behavior of the material. CONCR provided quite accurate pre-peak behavior results and peak strength values. Moreover, it was possible to plot the opening of cracks and those plots agreed with the experimental results. Nevertheless, as CONCR is suitable to reproduce brittle failures, it did not capture the long deformations characteristic of cob. Finally, the DMGE/DMGI proved to be inaccurate to reproduce both pre-peak and post-peak behavior. Although parameters could be calibrated to obtain the appropriate peak strength, neither stresses nor did strains correspond to what was observed in the experimental campaign.

Keywords: Non-linear, FEM, Cob, ANSYS

Introduction

Cob is an earthen construction technique used to build monolithic load-bearing walls. The loam, mixture of soil, water and straw, is placed wet in a horizontal layer which after being left to dry for some time is shaped with sharp instruments into its final form. New layers are placed in top of the previous one and the process is repeated until the desired wall height is reached.

Monolithic techniques have the advantage of not presenting weakness planes such as it is in the case of modular constructions (namely adobe or rammed earth). Cob's cohesion is provided mainly by the clay cementing properties and the added organic fibers such as straw or heather [1]. Despite the low compressive strength of cob, this material presents a relatively good performance regarding the shear strength. Moreover, cob appears to be more flexible in comparison with the other earthen construction techniques, since it presents a relatively ductile post-peak behavior due to the fibers added to the mixture [1].

Cob remaining buildings are of vernacular nature and can be found in eighteen European countries [2]. According to Hamard et al. only within Germany, France and the UK there are at least 200 000 cob buildings [3]. Furthermore, the bulk of remaining earthen buildings, cob included, is located within the dry climate regions of the world [4] and in total earthen buildings house at least 30 % of the world's population [5].

Despite its importance, cob has not received as much attention by researches as other earthen techniques such as adobe, rammed earth or compressed earth blocks (CEB). Therefore, cob's structural behavior is not yet fully understood, nor material constitutive models have been specifically developed to simulate cob's structural response. Moreover, neither standards are available for the design of new cob buildings nor for the conservation of existent ones. After an extensive research that involved 55 documents related with the normalization and standardization of earthen construction techniques around the world, Cid et al. [6] identified that none of them was specialized on providing guidance for cob.

The purpose of a non-linear model is to identify the peak strength of a structure and reproduce more accurately its pre-peak and post-peak behavior. By doing so, a better safety evaluation of existent buildings can be performed thus avoiding the implementation of over conservative intervention measures that may cause the loss of their authenticity. This paper aims at assessing the suitability of the constitutive material models available in one of the most popular FEM software in the market, ANSYS [7], to replicate the non-linear response of cob wallettes. The simulations are based on the experimental campaign and the numerical simulations performed previously by Miccoli et al. [1] which represent one of the most complete and detailed studies of cob at the moment.

Methodology

Miccoli et al. [8] determined experimentally the stress-strain curves of cob, as well as adobe and rammed earth, both under simple compression and under diagonal compression. They also reported the failure mechanisms and the crack patterns of the tested wallettes (see Figure 1). Pull-off test were also carried out to determine cob's tensile strength. All cob's mechanical properties determined by Miccoli et al. are summarized and presented in Table 1.

Their numerical simulations to describe cob's structural behavior consisted in 2D plane stress models. They implemented a macro-modelling approach with a TSRCM constitutive model and a multilinear definition of the stress-strain relationship for the compressive behavior with an initial linear segment of $0.3 f_c$ and a post peak segment with negative slope. An exponential relationship was employed for the tensile behavior [8]. The software used was Diana [9].

Miccoli's et al. tests were simulated in this paper using ANSYS [7]. The values for the geometry and material properties were adopted as those reported by them [8] to replicate as accurately as possible the non-linear response of cob observed during their experimental campaign. Three different material constitutive models were employed, MISO, CONCR, and DMGE/DMGI.

MISO, which stands for multilinear isotropic hardening, is a rate-independent plasticity model characterized by a Von Mises yield criterion [10], an associative flow rule, and an isotropic hardening in which the yield surface remains centered about its initial centerline and expands in size as the plastic strains develop [11]. It is supported by plane and solid finite elements. The stress strain multilinear behavior and the initial and subsequent yield surfaces for isotropic hardening plasticity are shown in Figure 2. MISO does not support the definition of negative

slopes for the stress-strain relationship. A post-peak horizontal curve was defined with constant stress equivalent to the compressive strength of cob reported in Table 1.

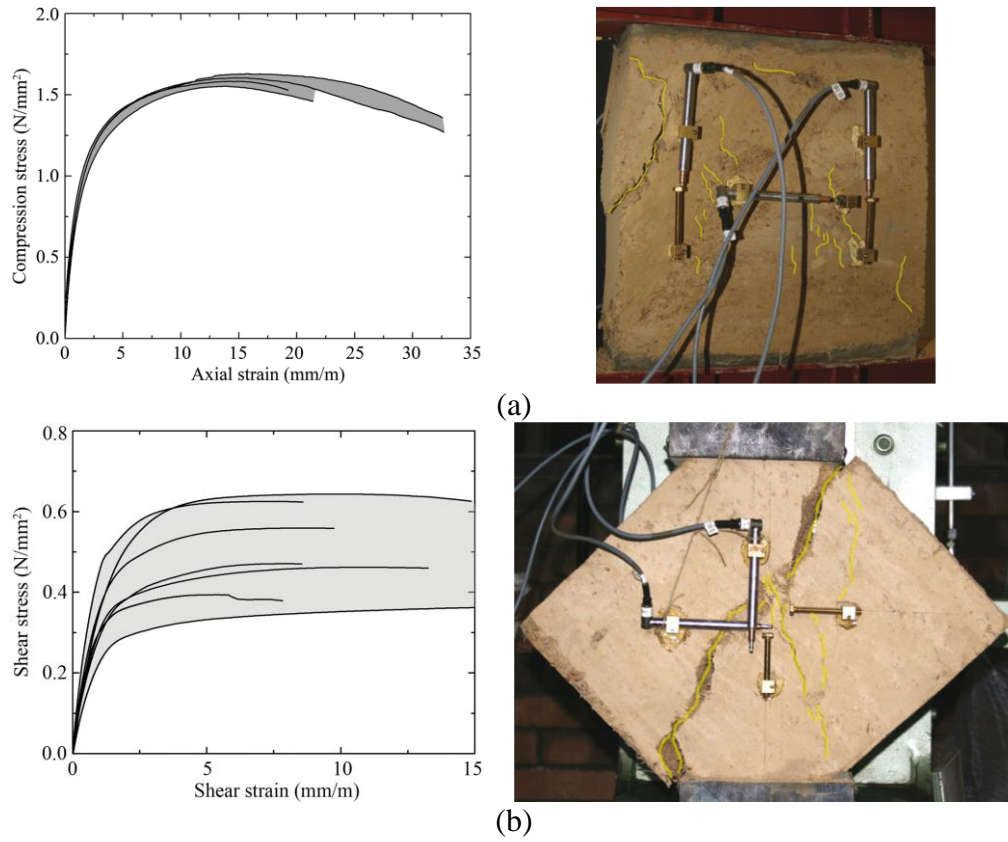


Figure 1. Stress-strain curves and crack patterns of cob wallettes under: (a) simple compression & (b) diagonal compression [8].

Table 1. Cob's mechanical properties [8].

Property	Value
Compressive strength f_c (MPa)	1.59
Tensile strength f_t (MPa)	$(0.10-0.16) f_c$
Tensile fracture energy (N/mm)	$(0.3-0.8) f_t$
Shear strength (MPa)	0.5 [1]
Shear modulus (MPa)	420 [1]
Modulus of elasticity (MPa)	1021
Poisson's ratio (-)	0.14
Density (kg/m^3)	1475

CONCR is a material constitutive model that can only be applied in combination with the legacy element called SOLID65 [10]. SOLID65 is an eight-node 3D element capable of cracking in tension and crushing in compression. It is suitable to model geological materials and reinforced composites [12]. The CONCR material model predicts the failure of brittle materials. The criterion for failure due to a multiaxial stress state can be expressed as follows:

$$\frac{F}{f_c} - S \geq 0 \quad (1)$$

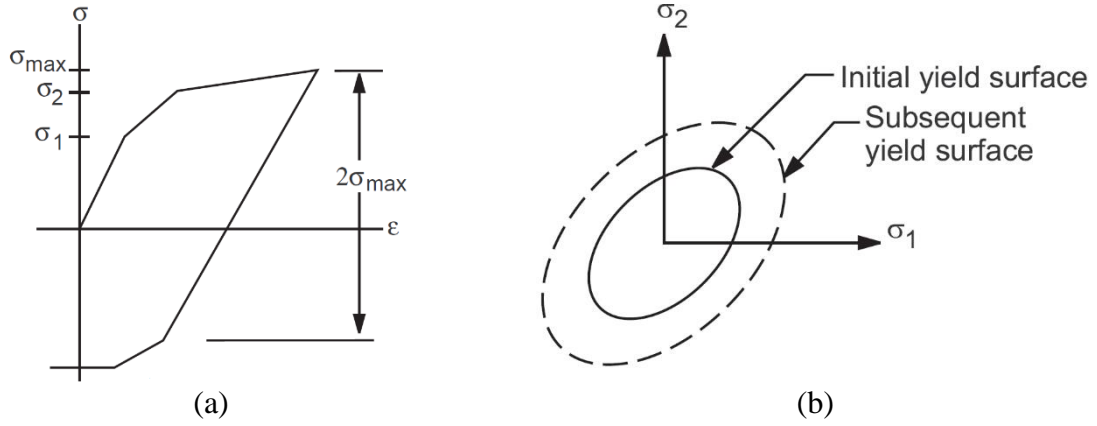


Figure 2. (a) Stress-strain multilinear isotropic behavior. (b) Initial and subsequent yield surfaces for isotropic hardening plasticity [11].

Where:

- F = Function of principal stress state ($\sigma_{xp}, \sigma_{yp}, \sigma_{zp}$).
- S = Failure surface expressed in terms of principal stresses and five input parameters:
 - f_c = Ultimate uniaxial compressive strength (taken from Table 1).
 - f_t = Ultimate uniaxial tensile strength (taken from Table 1).
 - f_{cb} = Ultimate biaxial compressive strength ($f_{cb} = 1.2f_c$).
 - f_1 = Ultimate compressive strength for a state of biaxial compression superimposed on hydrostatic stress state ($f_1 = 1.45f_c$).
 - f_2 = Ultimate compressive strength for a state of uniaxial compression superimposed on hydrostatic stress state ($f_2 = 1.725f_c$).

The presence of a crack at an integration point is represented through modification of the stress-strain relations by introducing a plane of weakness in a direction normal to the crack face. Also, a shear transfer coefficient β_t is introduced which represents a shear strength reduction factor for those subsequent loads which induce sliding (shear) across the crack face. If the crack closes, then all compressive stresses normal to the crack plane are transmitted across the crack and only a shear transfer coefficient β_c for a closed crack is introduced [11]. This condition can be seen in Figure 3. β_t , β_c and T_c , multiplier for amount of tensile stress relaxation, were calibrated to obtain a response from the wallettes as similar as possible to the one reported in the referenced experimental campaign (the values adopted were 0.25, 0.9 and 0.8 respectively).

If the material at an integration point fails in uniaxial, biaxial, or triaxial compression, the material is assumed to crush at that point. In SOLID65, crushing is defined as the complete deterioration of the structural integrity of the material [11]. To obtain a more detailed description of CONCR see [13].

DMGI, which stands for damage initiation, determines the onset of material damage under loading. It needs to be used in combination with DMGE, damage evolution, which defines the way in which the material degrades once the damage has started [10]. A Hashin criteria was adopted to determine the DMGI material model with a continuum damage mechanics method (not supported by any 3D finite element). This physical failure criteria accounts for four damage modes, namely, fiber tension (rupture), fiber compression (kinking), matrix tension (cracking), and matrix compression (crushing) [11].

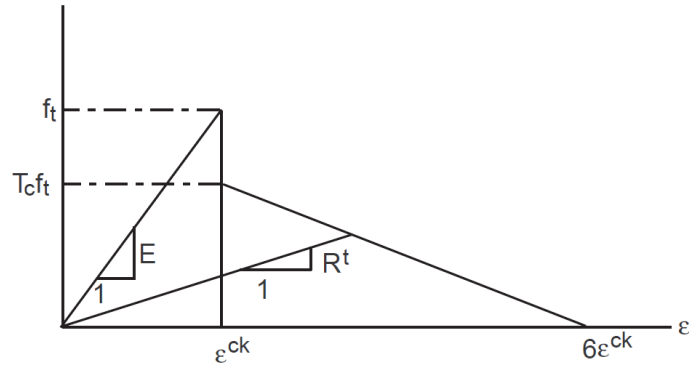


Figure 3. CONCR model for cracked condition [11].

For the continuum damage mechanics method damage variables increase gradually based on the energy amounts dissipated for the various damage modes. To achieve an objective response, the dissipated energy for each damage mode is regularized as follows [11]:

$$g_v = \frac{G_c}{L_e} \quad (2)$$

Where:

- g_v = Energy dissipated per unit volume.
- L_e = Characteristic length of the element calculated for the element area, A, as equal to:

$$L_e = \begin{cases} 1.12\sqrt{A}, & \text{for a square element} \\ 1.52\sqrt{A}, & \text{for a triangular element} \end{cases} \quad (3)$$

- G_c = Energy dissipated per unit area which for an specific damage mode is given by:

$$G_c = \int_0^{U_e^f} \sigma_e dU_e \quad (4)$$

Where:

- σ_e = Equivalent stress.
- U_e = Equivalent displacement.
- U_e^f = Ultimate equivalent displacement, where total material stiffness is lost for the specific mode.

Viscous damping coefficients η are also specified respectively for all four damage modes. For a specific damage mode, the damage evolution is regularized as follows [11]:

$$d'_{t+\Delta t} = \frac{\eta}{\eta + \Delta t} d'_t + \frac{\Delta t}{\eta + \Delta t} d_{t+\Delta t} \quad (5)$$

Where:

- $d'_{t+\Delta t}$ = Regularized damage variable at current time.
- d'_t = Regularized damage variable at the end of the last sub step.
- $d_{t+\Delta t}$ = Unregularized current damage variable.

Hashin's fiber and matrix failure criterion are described according to EQ. (6) and to EQ. (7) respectively.

$$\xi_4 = \begin{cases} \left(\frac{\sigma_x}{\sigma_{xt}^f} \right)^2 + \frac{\sigma_{xy}^2 + \sigma_{xz}^2}{(\sigma_{xy}^f)^2}, & \text{if } \sigma_x > 0 \\ \left(\frac{\sigma_x}{\sigma_{xc}^f} \right)^2, & \text{if } \sigma_x \leq 0 \end{cases} \quad (6)$$

$$\xi_5 = \begin{cases} \left(\frac{\sigma_y + \sigma_z}{\sigma_{yt}^f} \right)^2 + \frac{\sigma_{yz}^2 - \sigma_y \sigma_z}{(\sigma_{yz}^f)^2} + \frac{\sigma_{xy}^2 + \sigma_{xz}^2}{(\sigma_{xy}^f)^2} & \text{if } \sigma_y + \sigma_z > 0 \\ \frac{1}{\sigma_{yc}^f} \left(\left(\frac{\sigma_{yc}^f}{2\sigma_{yz}^f} \right)^2 - 1 \right) (\sigma_y + \sigma_z) + \left(\frac{\sigma_y + \sigma_z}{2\sigma_{yz}^f} \right)^2 + \frac{\sigma_{yz}^2 - \sigma_y \sigma_z}{(\sigma_{yz}^f)^2} + \frac{\sigma_{xy}^2 + \sigma_{xz}^2}{(\sigma_{xy}^f)^2} & \text{if } \sigma_y + \sigma_z \leq 0 \end{cases} \quad (7)$$

Orthotropic elasticity parameters, Young's modulus, Poisson's ratio and Shear modulus, were defined according to the values presented in Table 1 assuming same value for all directions (x, y and z). Similarly, orthotropic stress limits, tensile, compressive and shear, were assumed to have same value in all directions. Finally, the dissipated energy and viscous damping coefficients values used for the simulations are those presented in Table 2.

Table 2. Dissipated energy and viscous coefficient values for the DMGE/DMGI models.

Material constant	Meaning	Value
C1	Energy dissipated per unit area from tensile fiber damage (N/m).	1.0x10 ¹⁰
C2	Viscous damping coefficient for tensile fiber damage.	0.001
C3	Energy dissipated per unit area from compressive fiber damage (N/m).	1.0x10 ¹⁰
C4	Viscous damping coefficient for compressive fiber damage.	0.001
C5	Energy dissipated per unit area from tensile matrix damage (N/m).	1.035x10 ⁵
C6	Viscous damping coefficient for tensile matrix damage.	0.37
C7	Energy dissipated per unit area from compressive matrix damage (N/m).	7.950x10 ⁵
C8	Viscous damping coefficient for compressive matrix damage.	0.37

The values of the non-participating modes (C1 and C3) were set at a relatively high value to avoid their interference in the study of the cob typical damage modes, namely, cracking and crushing (C5 and C7), as advised in [14]. The values of the correspondent viscous damping coefficient for tensile and compressive fiber damage (C2 and C4) were randomly assigned as they are negligible. Whereas that those for tensile and compressive matrix damage (C6 and C8) were calibrated to obtain the reported peak strength in the simple compressive test.

The dimensions of the FEM models are shown in Figure 4. To simulate the compressive tests a displacement control approach was used. The steel plates in the bottom were fixed whereas that vertical displacements were applied to the plates on top of the wallettes. Self-weight was neglected. For the MISO model, large simulations were taken into account. On the other hand,

no large deformations were used for CONCR as advised in [12] as they would cause convergence problems. A summary of FEM simulations is presented in Table 3.

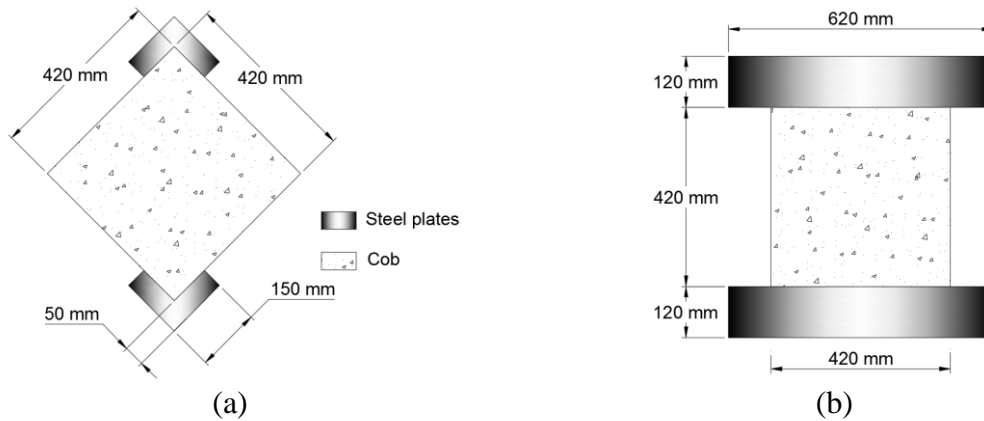


Figure 4. Dimensions used for: (a) diagonal compression and (b) simple compression simulations.

For the mesh sensitivity analysis, a mesh refinement method was selected. The maximum element size studied were 50, 30 and 10 mm. The element shape was verified with the mesh quality metrics provided by the software. Thanks to the relatively simple geometry of the models, the values for the average mesh quality were located between 0.86 and 0.99 for all simulations. Finally, the element type for each one of the simulations performed is indicated in Table 3.

Table 3. Finite element analyses set-ups.

Material	Geometry	Finite element (# of nodes)	Large deformations
MISO	2D	PLANE183 (8)	On
	3D	SOLID186 (20)	On
CONCR	3D	SOLID65 (8)	Off
DMGE/DMGI	2D	PLANE183 (8)	Off

Results and discussion

The results obtained from the simulations performed using ANSYS are presented in the form of stress-strain graphs and maximum principal stress plots. The upper and lower limits of the stress-strain graphs represent the experimental envelope reported by Miccoli et al. [8]. Besides, crack and crushing plots are shown for the CONCR models. Finally, a table is presented to show the mesh sensitivity using as reference the values obtained for the peak strengths of each simulation.

Plane stress and 3D simple compression stress-strain curves using MISO are shown in Figure 5 and Figure 6 respectively. The plane stress model reproduced quite accurately the pre-peak behavior of cob. Unfortunately, as this plasticity model is not capable to reproduce post-peak softening, it was not able to follow the loss of strength of the material after the maximum stress was attained. Regarding the mesh sensitivity, same behavior path was reproduced for the three element sizes. However, the finer the mesh the larger were the values obtained for the strains. The discrepancy values computed between the peak strengths obtained and the reference value are smaller than 10 % for the three mesh sizes implemented as can be seen in Table 4.

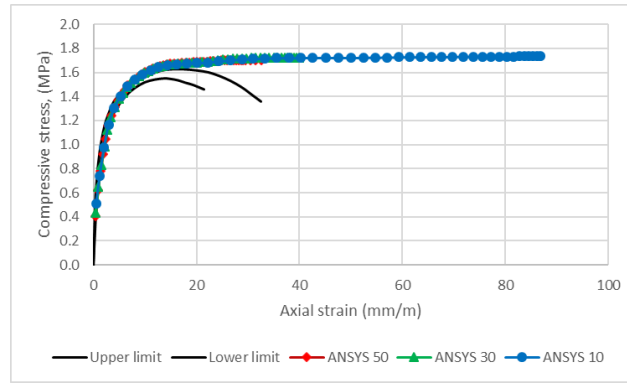


Figure 5. Plane stress simple compression stress-strain curves using MISO.

The 3D MISO model results were not as accurate as the ones obtained from the plane stress one. It presented a stiffer behavior and the plastic strains started to develop at a higher stress. The plots produced do not fit with the experimental ones. As 3D models include the Poisson's ratio effect in the orthogonal directions to the plane of the wall, the stress-strain multilinear curve used, which was calibrated with a plane stress simulation that neglects such effect, turns out to be inadequate. Table 4 presents discrepancy values for the peak strengths obtained for the 3D MISO model above 20 and 30 % with respect to the reference value for the different mesh sizes implemented.

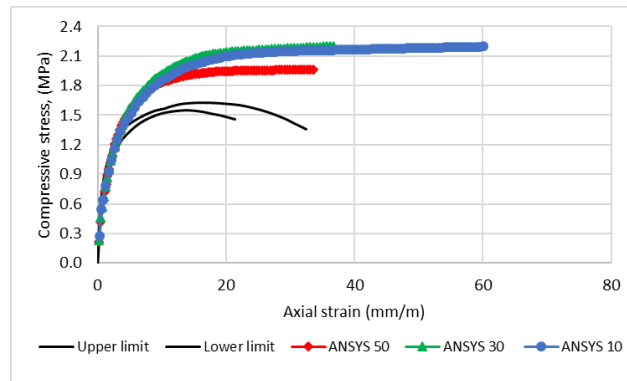
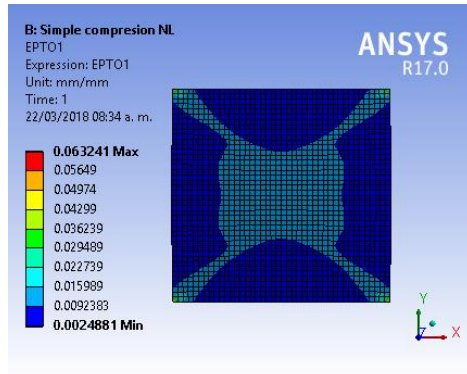


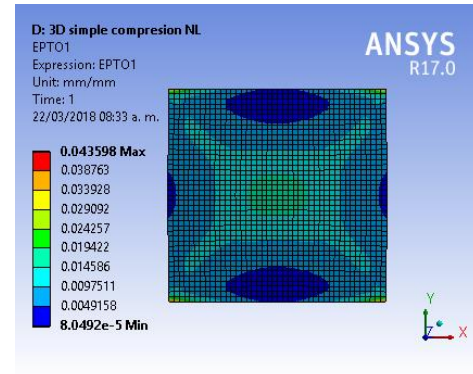
Figure 6. 3D simple compression stress-strain curves using MISO.

MISO models do not provide directly the appearance of cracks nor crushing within the material. As an indication for such failure modes the maximum principal strains, which are shown in Figure 7, can be interpreted (only the plots obtained for the 10 mm models are presented for the sake of brevity but similar patterns were found for the 30 and 50 mm models). As it can be seen, both plane stress and 3D models show a symmetric x pattern of the strains which is typical on simple compression tests of brittle materials and is considered as a satisfactory failure pattern [15].

The obtained stress-strain curves from the diagonal compression simulations are shown in Figure 8 and Figure 9 for the plane stress and 3D models respectively. Wider scattering was reported by Miccoli et al. for the shear response of the cob wallets as can be seen from the upper and lower limit curves. All plane stress MISO models fit within such limits. Unfortunately, the discrepancy values for the peak strengths are quite high, between 13 and 20 %, as can be seen in Table 4.



(a)



(b)

Figure 7. Maximum principal strains for the simple compression MISO models (a) plane stress & (b) 3D.

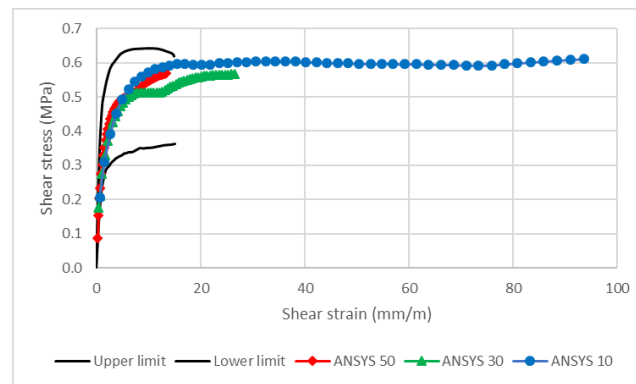


Figure 8. Plane stress diagonal compression stress-strain curves using MISO.

On the other hand, 3D MISO stress-strain curves do not fit within the reference range. These results are similar as those reported for the 3D MISO simple compression curves. A stiffer behavior can be observed which may be explained by the Poisson's ratio effect in the orthogonal directions of the wall plane for the 3D models. Moreover, an important difference between the finer mesh (10 mm) and the coarser ones (30 & 50 mm) can be seen. Discrepancy values for the peak strengths are within 39 and 41 % for the 30 and 50 mm models whereas that for the 10 mm model this value increases up to 76 % (see Table 4).

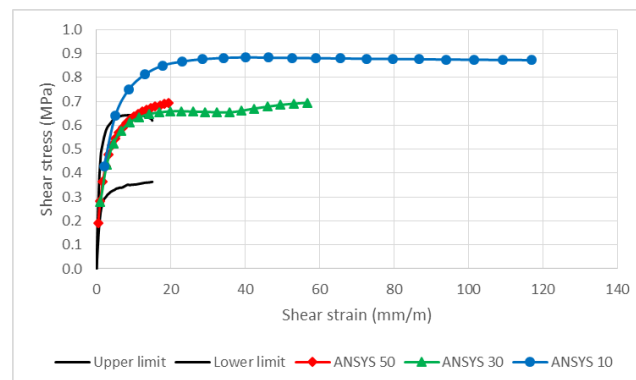


Figure 9. 3D diagonal compression stress-strain curves using MISO.

Figure 10 shows the maximum principal strains from the diagonal compression simulations. Due to the geometry of the models, singularity points appear at the contact between the sharpened

edges of the steel plates with the cob wallettes. These figures do not match with the failure pattern observed during the experimental campaigns and place serious doubts regarding the validity of the results obtained. In future work, those singularities must be removed by rounding the edges of the plates or by applying the displacements directly on the edge nodes of the cob wallettes.

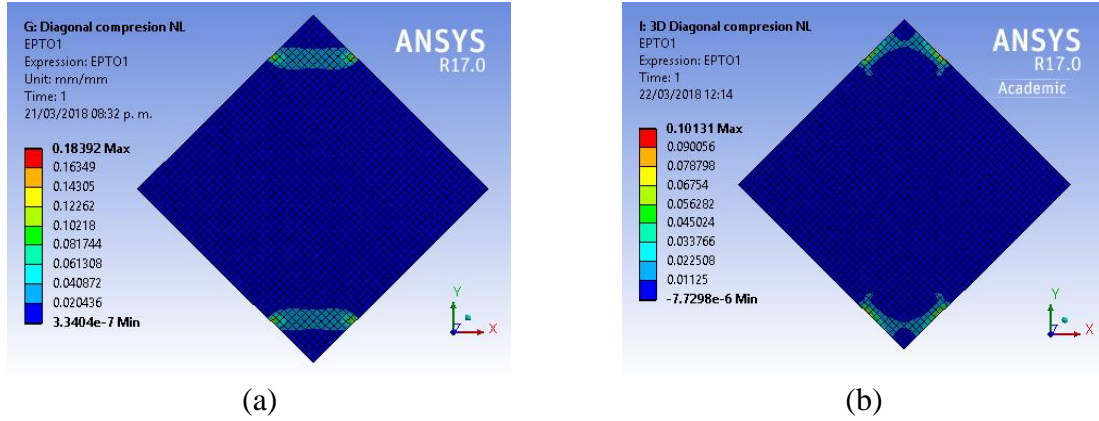


Figure 10. Maximum principal strains for the diagonal compression MISO models (a) plane stress & (b) 3D.

The stress-strain curves obtained with the CONCR model for the simple compression simulation are shown in Figure 11. They display a slightly stiffer pre-peak behavior in comparison with the experimental response of cob. Nonetheless, the overall behavior turned out to be quite accurate. Regarding the mesh sensitivity results, discrepancy values for the peak strengths were computed within 10 % for the three mesh sizes implemented.

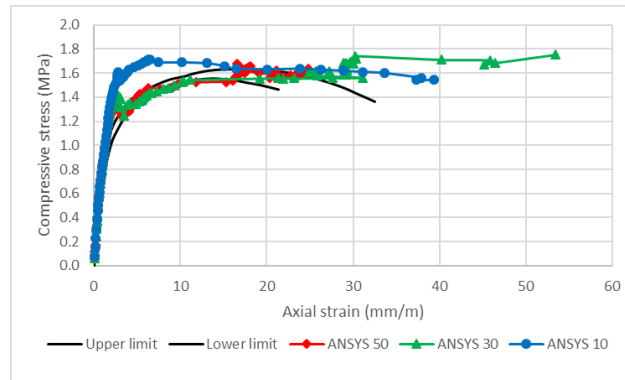
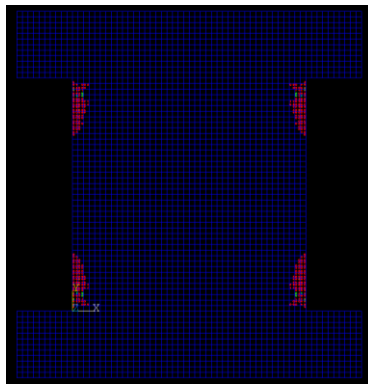


Figure 11: 3D simple compression stress-strain curves using CONCR.

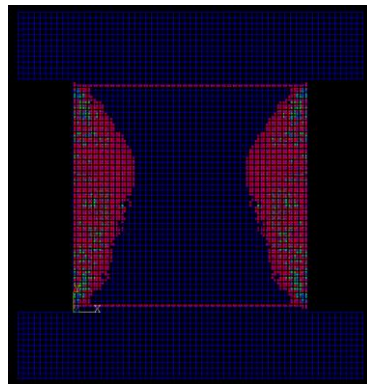
The CONCR material model, in combination with the finite element SOLID65, has the capability to represent cracks and/or crushing explicitly in a graphical way. Figure 12 shows those plots at three different stages of the simulation, namely, at substeps 40, 50 and 100 (last substep). It can be appreciated how the failure starts at the corners of the wallette (a), propagates to the center forming the typical cone shape of compression tests (b) and finally reaches the total damage of the material (c).

The simulation of the diagonal compression test with CONCR was more mesh sensitive as can be seen in Figure 13. None of the three models was capable to reproduce the post-peak ductile behavior of cob reported after the experimental campaign. Moreover, the models with 30 and 50 mm mesh size gave quite big discrepancy values regarding the peak strengths of around 47 %. On the other hand, the 10 mm model gave a very accurate peak strength value. Even though

it gave a relatively brittle post peak behavior, the values for the final strains are similar to those reported by Miccoli et al. This model represents the more accurate way to reproduce the non-linear behavior of cob from the three different material models studied in this paper.



(a)



(b)

ADD FIGURE OF
SUBSTEP 100!!!

(c)

Figure 12. Crack and crushing development for a simple compression test using CONCR; (a) at substep 40, (b) at substep 50, (c) at substep 100.

Regarding the failure pattern of the CONCR model, it can be seen from Figure 14 that cracks initially appear at the center of the wallette (a), then propagate diagonally in both directions (b) until they reach the faces of the wallette (c) forming the typical x pattern expected from a compression test.

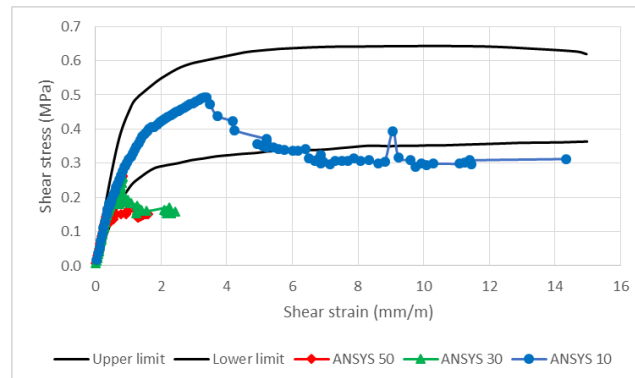


Figure 13. 3D diagonal compression stress-strain curves using CONCR.

Finally, the stress-strain curves and the maximum principal strain plots for the DMGE/DMGI models are presented in Figure 15 and Figure 16 respectively. Even though input parameters were calibrated to provide an accurate strength value for the simple compression test (see Figure 15 (a) and the mesh sensitivity values for the discrepancy of the peak strengths presented in Table 4), neither the pre-peak nor the post peak behavior of cob was captured properly. DMGE/DMGI material shows a stiffer pre-peak behavior and, after reaching the peak strength a, suddenly loss of strength. Thus, depicting a fully brittle material behavior rather than the progressive loss of capacity and ductile post peak behavior of cob. Furthermore, the shear responses from the simulations were far from replicating the cob performance reported by Miccoli et al. (see Figure 15 (b)).

As can be seen in Figure 16, neither the simple compression nor the diagonal compression maximum principal strains correspond with the expected x pattern considered as satisfactory. For the simple compression plot, strains accumulate at the interface between the steel plates and the top and bottom of the cob wallette. Whereas that for the diagonal compression plot,

strains accumulate at the singularity points between the sharpened edges of the steel plates in contact with the faces of the cob wallettes.

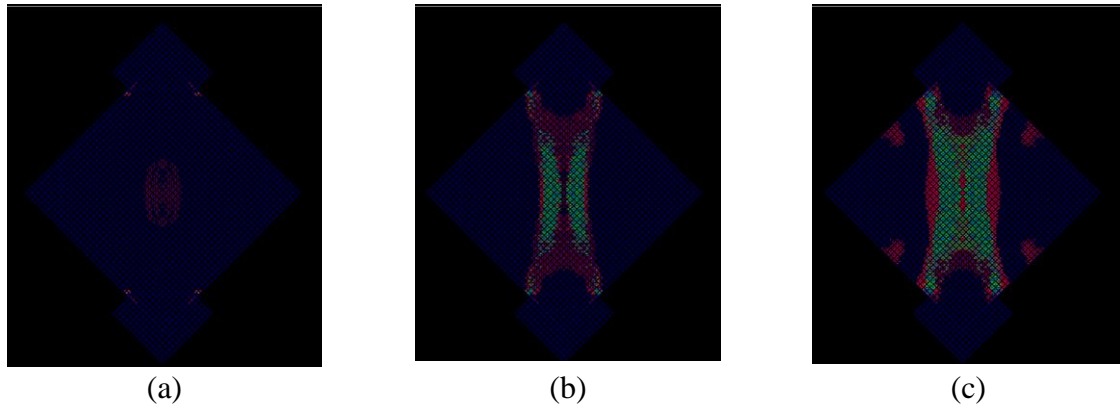


Figure 14. Crack and crushing development for a diagonal compression test using CONCR; (a) at sub step 50, (b) at sub step 70, (c) at sub step 100.

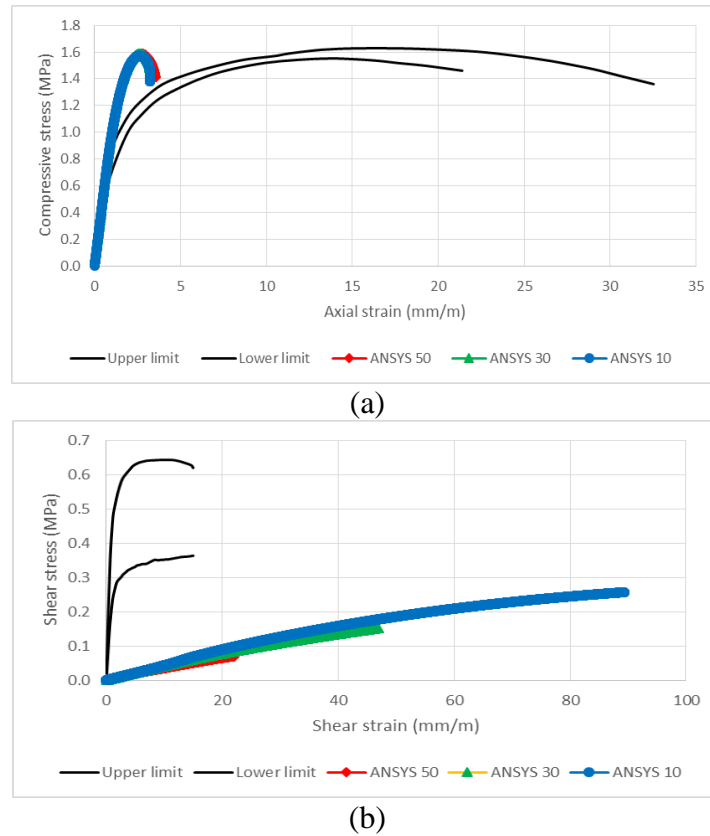


Figure 15. Plane stress stress-strain curves using DMGE/DMGI for (a) simple compression & (b) diagonal compression simulations.

As said before, the input parameters of the DMGE/DMGI models were calibrated to obtain the same peak strength as the reference for the simple compression test. Therefore, the discrepancy values are quite small (within 1 %). On the other hand, the discrepancy values for the for the peak strengths of the diagonal test are the higher ones among all set of simulations (going from 48 up until the 86 %). As neither pre-peak/post-peak behavior nor the distribution of the maximum principal strains correspond to the results obtained from the experimental campaign,

the DMGE/DMGI material models are the less suitable to reproduce cob's structural response among the set of three different material models implemented.

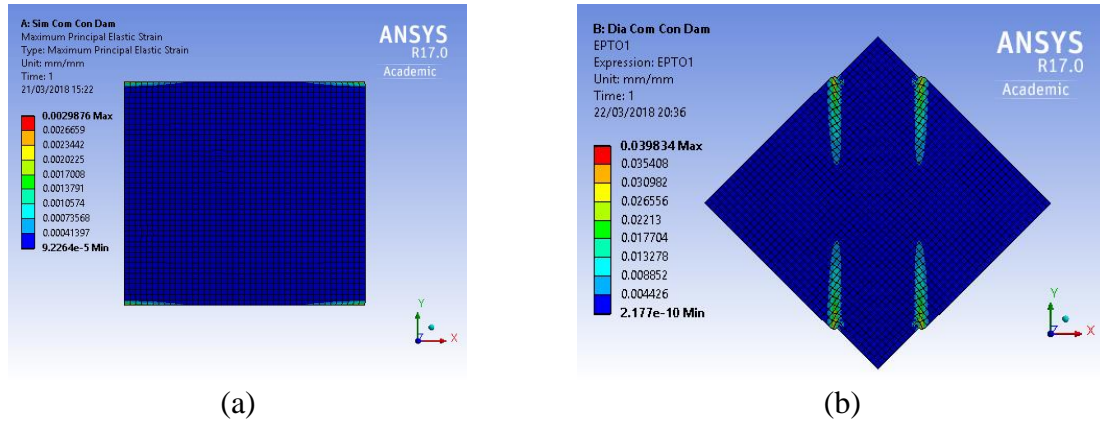


Figure 16. Maximum principal strains using DMGE/DMGI for (a) simple compression model & (b) diagonal compression model.

Table 4. Mesh sensitivity in terms of peak strengths.

Test	Model	Mesh size (mm)	Peak strength (MPa)	Reference value (MPa)	Discrepancy (%)
Simple compression	2D MISO	50	1.704	1.59	7.16
		30	1.722	1.59	8.28
		10	1.736	1.59	9.15
	3D MISO	50	1.965	1.59	23.60
		30	2.201	1.59	38.44
		10	2.196	1.59	38.08
	CONCR	50	1.680	1.59	5.67
		30	1.752	1.59	10.21
		10	1.714	1.59	7.81
	DMGE/DMGI	50	1.587	1.59	0.18
		30	1.587	1.59	0.21
		10	1.572	1.59	1.11
Diagonal compression	2D MISO	50	0.569	0.50	13.75
		30	0.566	0.50	13.27
		10	0.611	0.50	22.20
	3D MISO	50	0.706	0.50	41.26
		30	0.696	0.50	39.11
		10	0.883	0.50	76.55
	CONCR	50	0.263	0.50	47.36
		30	0.262	0.50	47.57
		10	0.492	0.50	1.70
	DMGE/DMGI	50	0.070	0.50	86.07
		30	0.152	0.50	69.64
		10	0.257	0.50	48.69

Conclusions

The suitability of the three constitutive material models (MISO, CONCR & DMGE/DMGI) available in ANSYS to replicate the non-linear response of cob wallettes was assessed. The simulations were based on results obtained from previous experimental campaigns.

MISO could reproduce the pre-peak behavior of cob and principal stresses could be used as an indication of the opening of cracks. On the other hand, it did not capture the softening post-peak behavior of the material. CONCR provided quite accurate pre-peak behavior results and peak strength values. Moreover, it was possible to plot the opening of cracks and those plots agreed with the experimental results. Nevertheless, as CONCR is suitable to reproduce brittle failures, it did not capture the long deformations characteristic of cob. Finally, the DMGE/DMGI proved to be inaccurate to reproduce both pre-peak and post-peak behavior. Although parameters could be calibrated to obtain the appropriate peak strength, neither stresses nor strains correspond to what was observed in the experimental campaign.

The model that better represented the behavior of cob was the 3D CONCR with a 10 mm mesh size. The discrepancy values for both simple and diagonal compression peak strengths are smaller than 10 %. Moreover, the cracks obtained in the model are in good agreement with the typical failure pattern presented in these types of experimental tests.

References

1. Miccoli, L., U. Müller, and P. Fontana, *Mechanical behaviour of earthen materials: a comparison between earth block masonry, rammed earth and cob*. Construction and building materials, 2014. **6**: p. 327 - 339.
2. Terra Incognita, *Terra Europae, Earthen Architecture in the European Union* ed. E. ETS. 2011.
3. Hamard, E., et al., *Cob, a vernacular earth construction process in the context of modern sustainable building*. Building and environment, 2016. **106**: p. 103-119.
4. Piesik, S., *Habitat: Vernacular Architecture for a Changing Planet*. 2017, UK: Thames & Hudson Ltd.
5. Keefe, L., *Earth building : methods and materials, repair and conservation*. 2005, London: Taylor & Francis. xii, 196 p.
6. Cid, J., F.R. Mazarron, and I. Canas, *The earth building normative documents in the world*. Informes de la CConstruccion, 2011. **63**(523): p. 159-169.
7. ANSYS®, *ANSYS® Academic Research Mechanical*. 2017.
8. Miccoli, L., et al., *In-plane behaviour of earthen materials: a numerical comparison between adobe masonry, rammed earth and cob*, in *6th ECCOMAS Thematic Conference on Computational Methods in Structural Dynamics and Earthquake Engineering* M. Papadrakakis and M. Fragiadakis, Editors. 2017: Rhodes Island, Greece.
9. DIANA, *TNO DIANA*. 2014, TNO DIANA BV: Delft, The Netherlands.
10. ANSYS Inc., *ANSYS Mechanical APDL Material Reference*. 2013.
11. ANSYS Inc., *ANSYS Mechanical APDL Theory Reference*. 2013.
12. ANSYS Inc., *ANSYS Mechanical APDL Element Reference*. 2013.
13. William, K. and E. Warnke, *Constitutive model for the triaxial behaviour of concrete*, in *Seminar on concrete structures subjected to triaxial stresses*. 1974: Bergamo, Italy.
14. Barbero, E.J. and M. SHahbazi, *Determination of material properties for ANSYS progressive damage analysis of laminated composites*. Composite structures, 2017. **176**: p. 768-779.
15. British Standard, *BS EN 12390-3:2009 Testing of hardening concrete, Part 3: Compressive strength of test specimens*. 2009.